

# Recombination Kinetics in Organic-Inorganic Perovskites: Excitons, Free Charge, and Subgap States

Samuel D. Stranks,<sup>1</sup> Victor M. Burlakov,<sup>2</sup> Tomas Leijtens,<sup>1</sup> James M. Ball,<sup>1</sup> Alain Goriely,<sup>2</sup> and Henry J. Snaith<sup>1,\*</sup>

<sup>1</sup>*Department of Physics, University of Oxford, Parks Road, Oxford, OX1 3PU, United Kingdom*

<sup>2</sup>*Mathematical Institute, OCCAM, University of Oxford,  
Woodstock Road, Oxford, OX2 6GG, United Kingdom*

(Received 14 August 2014; published 11 September 2014)

Organic-inorganic perovskites are attracting increasing attention for their use in high-performance solar cells. Nevertheless, a detailed understanding of charge generation, interplay of excitons and free charge carriers, and recombination pathways, crucial for further device improvement, remains incomplete. Here, we present an analytical model describing both equilibrium properties of free charge carriers and excitons in the presence of electronic subgap trap states and their time evolution after photoexcitation in  $\text{CH}_3\text{NH}_3\text{PbI}_{3-x}\text{Cl}_x$ . At low fluences the charge-trapping pathways limit the photoluminescence quantum efficiency, whereas at high fluences the traps are predominantly filled and recombination of the photogenerated species is dominated by efficient radiative processes. We show experimentally that the photoluminescence quantum efficiency approaches 100% at low temperatures and at high fluences, as predicted by our model. Our approach provides a theoretical framework to understand the fundamental physics of perovskite semiconductors and to help in designing and enhancing the material for improved optoelectronic device operation.

DOI: 10.1103/PhysRevApplied.2.034007

## I. INTRODUCTION

The recent unprecedented increase in perovskite solar-cell efficiency suggests that organic-inorganic metal-halide perovskites may be the required “disruptive” technology to deliver widespread affordable solar power [1,2]. These perovskites exhibit not only strong absorptions across the solar spectrum [3,4], but also efficiently transport photoexcited species, with electron and hole diffusion lengths much longer than the film thickness required for complete light absorption [5,6]. Device power-conversion efficiencies have exceeded 16% in architectures where nanostructured electrodes are infiltrated with a perovskite absorber [7–10] and even when the perovskites are incorporated into simple planar heterojunction architectures [11–17]. Despite the rapid increase in device performance, there are only a handful of reports on the fundamental properties of the materials [5,18–26].

The usefulness of a semiconductor as a solar-cell material largely depends upon its ability to generate free charge carriers, have low electronic disorder, and sustain a large density of charge carriers under continuous illumination. The latter is proportional to the electron lifetime, which is strongly influenced by the mode and means of electron and hole recombination. The recombination rate  $\Gamma$  of electrons and holes is proportional to the rate at which electron and holes meet each other and the probability of

subsequent recombination versus separation. The Langevin theory for recombination stipulates that  $\Gamma$  is proportional to the product of the electron and hole number density ( $n_e \times n_h$ ) times a coefficient,  $\gamma$  (or  $R_{eh}$ ), which takes into account the charge mobility and dielectric properties of the semiconductor [27,28]. If the electron and hole number densities  $n_e$  and  $n_h$ , respectively, vary comparably, then  $\Gamma$  scales as  $n_e^2$ , and recombination is termed bimolecular. If  $n_h$  is approximately constant, for example, due to  $p$  doping in excess of the photogenerated free-carrier density,  $\Gamma$  scales proportionally to  $n_e$ , and recombination is termed monomolecular. Wehrenfennig *et al.* find that bimolecular recombination rates in these materials are 4 orders of magnitude lower than expected from the Langevin theory [24]. Deschler *et al.* demonstrated a bimolecular photoluminescence (PL) decay in  $\text{CH}_3\text{NH}_3\text{PbI}_{3-x}\text{Cl}_x$ , suggesting that recombination of free electrons and holes is responsible for radiative decay, although near-monomolecular recombination is observed at low excitation fluences, which remains unexplained [20]. Remarkably, these three-dimensional perovskites have been found to be highly emissive, and lasing has been observed at room temperature [20,23,29]. The thermal generation of free charge and low levels of nonradiative recombination are critical properties if perovskite solar cells are to approach the Shockley-Queisser efficiency limit, where detailed balance stipulates that all recombination is radiative [30]. However, the photoluminescence quantum efficiency (PLQE) is maximized at high excitation intensities, suggesting dominance of nonradiative decay pathways [23] under typical charge densities present during

\*Corresponding author.

h.snaith1@physics.ox.ac.uk

solar-cell operation. Determining the origin of the non-radiative decay and a detailed understanding of charge generation and exceptionally slow recombination within perovskite absorbers are essential both to further our understanding and to reach the ultimate potential for these materials in both photovoltaic and light-emitting applications.

Here, we combine PL measurements from pulsed and continuous excitation of  $\text{CH}_3\text{NH}_3\text{PbI}_{3-x}\text{Cl}_x$  thin films with a theoretical model. We find that at low excitation fluences, including those relevant to solar cells, the evolution of photoexcited species is significantly affected by electronic traps. At high excitation fluences, when all the traps become filled, the evolution is dominated by radiative bimolecular recombination. Our model also predicts the ratio between exciton and free charge populations, which deviates considerably from classical thermodynamic considerations, which do not account for traps and “photodoped” carriers.

## II. RESULTS AND DISCUSSION

Thin (approximately 260 nm)  $\text{CH}_3\text{NH}_3\text{PbI}_{3-x}\text{Cl}_x$  perovskite films are solution-processed on glass [5] (see Supplemental Material for experimental methods [31]). The PL spectrum of the perovskite [Fig. 1(a)] is centered at the onset of the absorption spectrum, which is characteristic for direct band-gap semiconductors [5,22]. Upon illumination [Fig. 1(b)], the PL rises slowly over a time scale of seconds. This time scale matches the rise in the open-circuit voltage of a complete planar heterojunction perovskite solar cell upon illumination with simulated (air mass 1.5) sunlight [Fig. 1(b)], suggesting that the same mechanism is involved and justifies the relevance of PL to solar cells. We postulate that there is a distribution of subgap trap states. These slow rises are consistent with a slow filling and stabilization of these charge trap states by injected or photogenerated electrons, raising the quasi-Fermi-level for electrons (and hence  $V_{\text{OC}}$ ) and reducing the availability of trap sites to mediate nonradiative recombination. The very slow rise times may be indicative that ionic motion (presumably halide or methylammonium) is also contributing to the reduction in trap site density over time under illumination or to stabilization of the trapped charge.

To probe the depopulation of trap states, we monitor the transient voltage decay of a device following a perturbing pulse (0.1–1  $\mu\text{s}$ ) by using a method described previously [32,33] [Fig. 1(c)]. The sample is held at low steady-state background light bias (0.01 sun equivalent) to ensure availability of trap states prior to the perturbing pulse, as seen by observing that the voltage (i.e., quasi-Fermi-level in the perovskite) in this experiment is in the same range as that in which trap filling seems to dominate the voltage rise upon illumination [Fig. 1(b)]. We observe a fast initial component that approaches the system resolution (time constant of approximately 10  $\mu\text{s}$ ) and a long tail

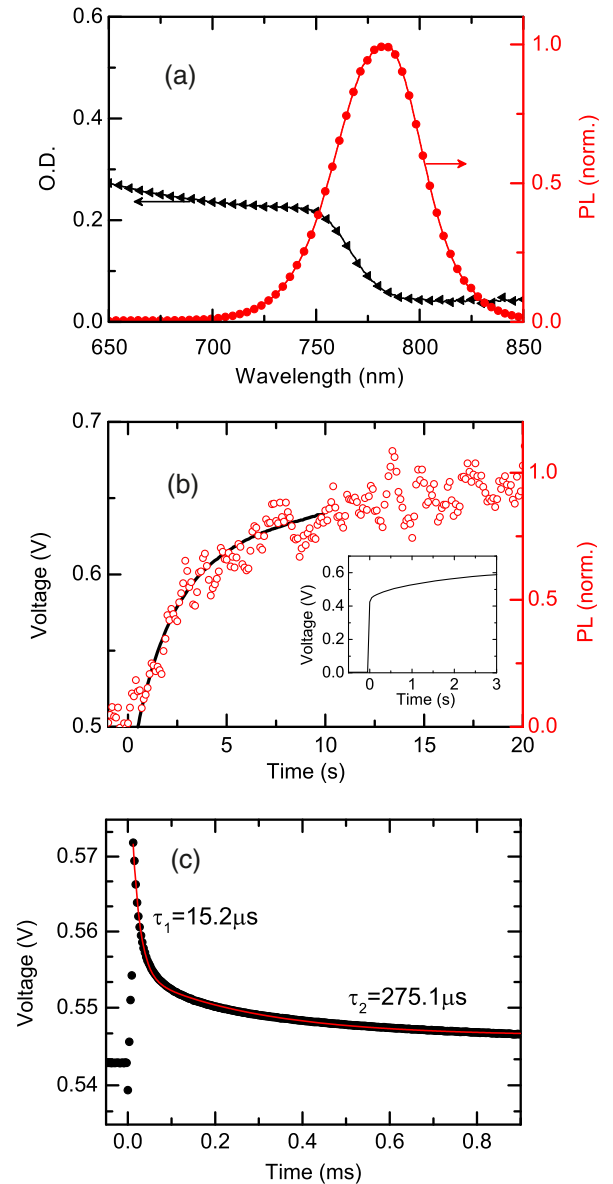


FIG. 1. (a) Absorption spectrum, and steady-state PL spectrum when photoexcited by a cw 532-nm laser, of a perovskite sample. (b)  $V_{\text{OC}}$  rise over time (black line) following illumination of a full device with an intensity approximately equivalent to full sunlight from a white-light LED array source, matching the PL rise over time (red data) for a flat film photoexcited with an equivalent intensity to full sunlight (532-nm cw laser, approximately 60  $\text{mW}/\text{cm}^2$ ). (c)  $V_{\text{OC}}$  decay following a perturbing pulse (equivalent to approximately 1 sun intensity) for a device under a low white-light bias (0.01 sun equivalent). A biexponential fit to the data is shown in red and time constants reported on the plot.

(approximately 100  $\mu\text{s}$ –1 ms), the latter of which may be related to the time scale for trap depopulation.

In order to probe the postulation that the trap sites strongly influence the PL and device characteristics, we develop a model taking into account the time and temperature dependence of the PL. Here, we consider only

electronic traps, though the same formalism holds for hole traps. Under the steady state, i.e., when the PL signal has reached a constant value, an optical pulse excitation generates an electron-hole pair density of  $N(0)$ . There are  $N_T$  electron traps,  $n_T$  of which are filled, leaving  $n_T$  free “photodoped” holes in the valence band such that the concentration of free holes at each point in time is  $n_h = n_e + n_T$ , where  $n_e$  is the concentration of free photogenerated electrons. The total concentration of photo-generated species  $N = n_e + n_x$  is thus comprised of concentrations of free electrons and excitons  $n_x$  but excludes trapped electrons and corresponding photodoped holes.

In Fig. 2(a), we show transient PL decays at room temperature over a range of pulse fluences. We note that the sample is illuminated at each fluence until a steady transient emission is achieved. The shape of the decays is nearly monoexponential at relatively low excitation fluence but deviates significantly from monoexponential at higher fluence. We describe this behavior with the aid of the schematics in Fig. 2(c): In the steady state, there are many holes already present in the system as “background” or photodoped charges, because some of the electronic traps are filled. The degree of photodoping can be rather high even at low excitation levels due to a very low depopulation rate  $R_{\text{dep}}$  of trapped electrons [Fig. 1(c)]. When the sample is photoexcited with a low fluence, the concentration of photoinduced electrons is much lower than the total concentration of free holes [since  $n_h(t) = n_e(t) + n_T(t)$ ,  $n_e \ll n_T$ ], and the recombination of electrons is almost monomolecular, since the additional photoexcited charge does not noticeably change the concentration of holes. If the excitation fluence is high enough, such that the concentrations of photoexcited electrons and holes from the laser pulse become comparable to the photodoped hole density [ $n_e(0) > n_T \sim N_T$ ], then the electron-hole recombination is bimolecular, resulting in a power-law decay until the free-electron concentration drops below the photodoped hole density, after which the decay again becomes monoexponential.

A generic kinetic model, accounting for exciton formation, dissociation into free charges, and trapping of free electrons, is given by the rate equations [31]

$$\frac{dn_e}{dt} = \frac{I}{d} + R_d n_x - R_f n_e n_h - R_{eh} n_e n_h - R_{\text{pop}} n_e (N_T - n_T), \quad (1)$$

$$\frac{dn_x}{dt} = R_f n_e n_h - R_d n_x - R_x n_x, \quad (2)$$

$$\frac{dn_T}{dt} = R_{\text{pop}} (N_T - n_T) n_e - R_{\text{dep}} (n_T^2 + n_T n_e). \quad (3)$$

The parameters  $R_f$ ,  $R_d$ , and  $R_x$  are the rates of exciton formation, dissociation, and decay, respectively.  $R_{eh}$ ,  $R_{\text{pop}}$ ,

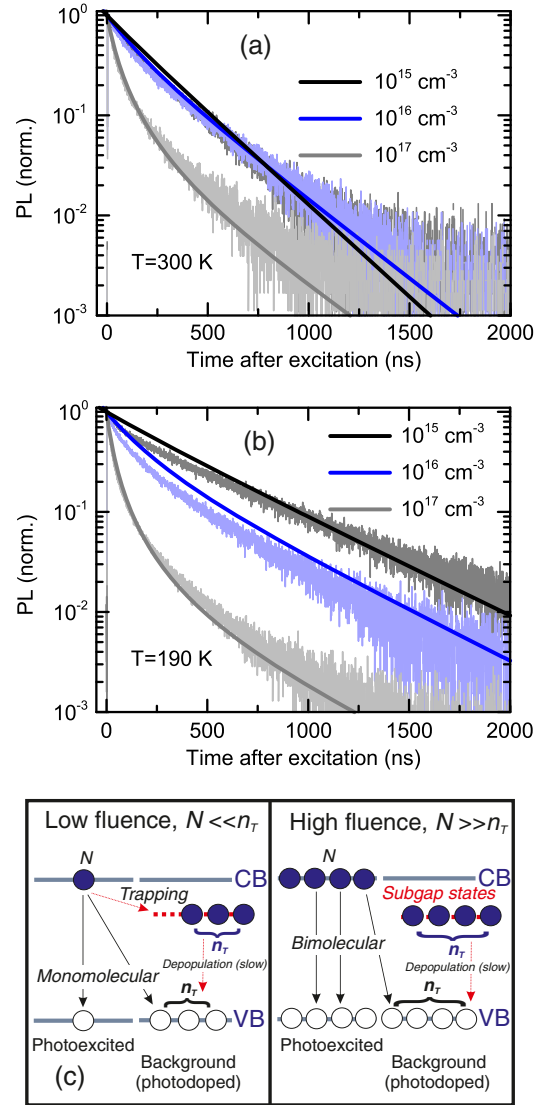


FIG. 2. (a),(b) PL decays detected at 780 nm from perovskite samples at (a) 300 and (b) 190 K, following pulsed excitation (510 nm, 300-kHz repetition rate) with different initial photoexcitation densities  $N(0)$ . Solid lines are fits from the model. (c) Schematic to illustrate recombination mechanisms for the low- and high-fluence regimes. We note that there is likely to be a distribution of states at different subgap energies, but they are shown here at a single energy for simplicity.

and  $R_{\text{dep}}$  determine the recombination rate of free electrons and holes, trap population, and depopulation by electrons, respectively, where depopulation is exclusively by recombination with either free (photogenerated) or photodoped holes and we assume the traps are deep enough to inhibit thermal detrapping to the conduction band;  $I$  is the excitation intensity,  $d$  is the film thickness, and  $N_T$  is the total trap concentration. Before solving this model, we make two further simplifications. (i) According to PL [Fig. 1(b)] and device [Figs 1(b) and 1(c)] measurements, the accumulation of charges in traps and their depopulation

take place on a time scale of milliseconds to seconds, suggesting that the trap concentration  $n_T$  can be taken as constant when we consider PL decays on time scales of microseconds. Therefore, on the time scales for the evolution of  $n_e$  or  $n_x$ , we set  $n_T = \text{const.}$  (ii) Because of the very fast exciton formation and dissociation, the free carriers and excitons can be assumed to be in thermal equilibrium throughout the entire PL decay. Indeed, the exciton dissociation rate, producing free carriers, can be estimated as  $P_{\text{diss}} = \nu \exp[-\frac{E_b}{k_B T}] \approx 10^{12} \text{ s}^{-1}$  (at room temperature  $T$ ), where we use  $E_b \sim 50 \text{ meV}$  [21,34–36] for the exciton binding energy,  $\nu = E_b/h \sim 10^{13} \text{ s}^{-1}$  is the attempt frequency ( $h$  is Planck's constant [37]), and  $k_B$  is the Boltzmann constant. Estimated exciton formation rates are on the order of approximately  $10^{10}$ – $10^{12} \text{ s}^{-1}$  [38,39]. These estimates provide a general picture of the dynamic equilibrium for photogenerated species in the perovskite film: Excitons are constantly dissociating to produce free charges, while free charges are associating to form excitons. A simple comparison between the dissociation time and the PL decay lifetime leads to the estimate that each charge undergoes approximately 10 000 exciton formation and dissociation events within its lifetime of approximately 100 ns [5]. Similar results to those presented below are also obtained when using exciton binding energy values on the lower end of those reported for these materials (approximately 15 meV [40]; see Supplemental Material Figs. S10–12 [31]).

The equilibrium between free carriers and excitons allows us to express the concentrations  $n_e$ ,  $n_h$ , and  $n_x$  in terms of the total (untrapped) photogenerated species density  $N$  as

$$\begin{aligned} n_h &= -\frac{(A - n_T)}{2} + \frac{1}{2} \sqrt{(A + n_T)^2 + 4AN}, \\ n_e &= n_h - n_T, \quad n_x = N - n_e, \end{aligned} \quad (4)$$

where  $A = \frac{v_x}{v_h v_e} \exp[-E_b/k_B T]$  and  $v_i = \lambda_i^3$ ,  $\lambda_i$  is the thermal wavelength of the species  $i$ , and Eq. (2) is now satisfied. Equation (4) represents a generalized version of the Saha equation [21,38,41] for  $p$ -type doped semiconductors (the  $n$ -doped case is obtained by interchanging the  $e$  and  $h$  subscripts). The equation for the evolution of normalized photogenerated species concentration  $x = N/(A + n_T)$ , after the pulsed excitation ( $I = 0$ ), takes the form

$$\begin{aligned} \frac{dx}{dt} &= -\frac{A\gamma_0 x}{A + n_T} \left[ x + \frac{n_T}{A} + \frac{R_{\text{pop}}(N_T - n_T)}{\gamma_0} \right], \\ \gamma_0 &= AR_{eh} + R_x, \end{aligned} \quad (5)$$

where  $\gamma_0$  is the total rate of electronic decay not involving traps.

The solution to this equation is

$$\begin{aligned} x &= \frac{C_1 x_0 \exp[-\gamma t]}{C_1 + x_0(1 - \exp[-\gamma t])}, \\ \gamma &= \frac{n_T \gamma_0}{A + n_T} + \frac{AR_{\text{pop}}(N_T - n_T)}{A + n_T}, \\ C_1 &= \frac{n_T}{A} + \frac{R_{\text{pop}}(N_T - n_T)}{\gamma_0}, \end{aligned} \quad (6)$$

with  $x_0 = N(t = 0)/(A + n_T)$ .

The description is completed by rewriting Eq. (3) for the concentration of filled traps (and therefore photodoped holes)  $n_T$  [31]:

$$\begin{aligned} n_T &= -\frac{1}{2}\alpha + \frac{1}{2}\sqrt{\alpha^2 + 4\beta N_T}, \\ \alpha &= \frac{[A + \frac{R_{\text{pop}}}{R_{\text{dep}}}(A - N_T)]}{(1 + \frac{1}{K} + \frac{R_{\text{pop}}}{R_{\text{dep}}})}, \\ \beta &= \frac{R_{\text{pop}}A}{R_{\text{dep}}(1 + \frac{1}{K} + \frac{R_{\text{pop}}}{R_{\text{dep}}})}, \end{aligned} \quad (7)$$

where  $K = \frac{1}{\gamma_0} \ln[1 + \frac{AN(0)}{N_T(A + N_T)}]$ . The normalized PL intensity is then

$$\begin{aligned} \frac{I_{eh}(t)}{I_{eh}(0)} &= \frac{I_{ex}(t)}{I_{ex}(0)} \\ &= \frac{n_e(t)n_h(t)}{n_e(0)n_h(0)} \\ &= \frac{1}{(n_T + Ax_0)Ax_0} \left( n_T + \frac{AC_1 x_0 \exp[-\gamma t]}{C_1 + x_0(1 - \exp[-\gamma t])} \right) \\ &\quad \times \frac{AC_1 x_0 \exp[-\gamma t]}{C_1 + x_0(1 - \exp[-\gamma t])}, \end{aligned} \quad (8)$$

We iteratively and globally fit the model to our experimental PL decays and PLQE data for the remaining parameters [31]. The fit to the time-resolved PL decays at 300 K shown in Fig. 2(a) leads to the parameter values  $R_{\text{pop}} = 2 \times 10^{-10} \text{ cm}^3 \text{ s}^{-1}$ ,  $R_{\text{dep}} = 8 \times 10^{-12} \text{ cm}^3 \text{ s}^{-1}$ ,  $N_T = 2.5 \times 10^{16} \text{ cm}^{-3}$ , and  $\gamma_0 = 1.4 \times 10^7 \text{ s}^{-1}$ , which accurately capture the range of the experimental data. We note that the extracted trap density  $N_T$  agrees well with results obtained by Xing *et al.* [23]. This trap density corresponds to one trap site for every approximately  $10^6$  unit cells, which is remarkably low for low-temperature solution-processed films [42,43].

Figure 2(b) shows the time-resolved PL decays at low temperature (190 K) as a function of excitation fluence (see Supplemental Material Fig. S4 for 250 K [31]). In order to provide reasonable fits to the data, we assume that the total trap concentration  $N_T$  also varies with temperature (see Supplemental Material Fig. S6 [31]). The fits in

Fig. 2(b) are shown with a total trap concentration  $N_T = 0.9 \times 10^{16} \text{ cm}^{-3}$ , which is a factor of approximately 3 lower than at 300 K ( $N_T = 2.5 \times 10^{16} \text{ cm}^{-3}$ ). This result suggests that the trap states are intrinsic to the perovskite and vary with temperature. We speculate that the traps are due to thermally activated atomic vacancies, a common type of point defect in perovskite structures [44–46]. In addition, the trap population rate at 190 K is the same as at 300 K ( $R_{\text{pop}} = 2 \times 10^{-10} \text{ cm}^3 \text{ s}^{-1}$ ), but the depopulation rate is slowed by a factor of approximately 4 ( $R_{\text{dep}} = 2 \times 10^{-12} \text{ cm}^3 \text{ s}^{-1}$ ) such that, for a given excitation density, more traps are filled and there are also less of them at low temperature.

Next, we consider continuous wave (cw) excitation. Equation (1) can be solved numerically when  $I \neq 0$  in the steady state to obtain the resulting photogenerated species density  $N$  and total filled trap concentration  $n_T$  in a perovskite film for a given incident intensity [Fig. 3(a)]. We note here that, under continuous excitation equivalent to solar fluences (dashed line), recombination in the perovskite is in the monomolecular regime ( $N \sim 10^{15} \text{ cm}^{-3} \ll n_T \sim 10^{16} \text{ cm}^{-3}$ ). The system transitions only at high excitation intensities ( $>100$  suns equivalent) to a bimolecular regime, in which recombination is no longer limited by traps. This finding implies that perovskite solar cells have not yet reached their full potential under operating conditions [30].

In Fig. 3(b), we show the steady-state concentration of excitons  $n_x$  as a function of total photogenerated species  $N$  at different temperatures. The dashed lines correspond to the case without subgap states (no photodoping), which is analogous to the results obtained by D’Innocenzo *et al.* using the Saha equation [21,41]. Our results deviate from those of the undoped material, meaning that even low levels of trap states can have a strong influence upon the exciton concentration. Nevertheless, it is clear that the dominant species are free charges ( $\leq 10\%$  excitons) under operating conditions in a perovskite device at 300 K (below approximately  $10^{15} \text{ cm}^{-3}$ ). Only at higher charge densities or low temperatures do we see larger fractions of excitons.

In Fig. 3(c), we show the experimental steady-state PLQE data as a function of charge density [49]. The PLQE increases with excitation intensity. This increase is due both to an increased filling of trap states and, possibly, to an increasing excitonic fraction of photogenerated species [Fig. 3(b)]. In addition, for a given excitation intensity, the PLQE increases as the temperature decreases (inset), reaching approximately 95% at about 190 K. This result shows that radiative recombination processes are dominant at low temperature, and it is consistent with the earlier results that, at low temperature, there are less traps and more of them are filled for a given excitation intensity. It is also consistent with an increased excitonic fraction at low temperature, which we could assume cannot be trapped within the Coulomb radius of a charged trap state (e.g., if

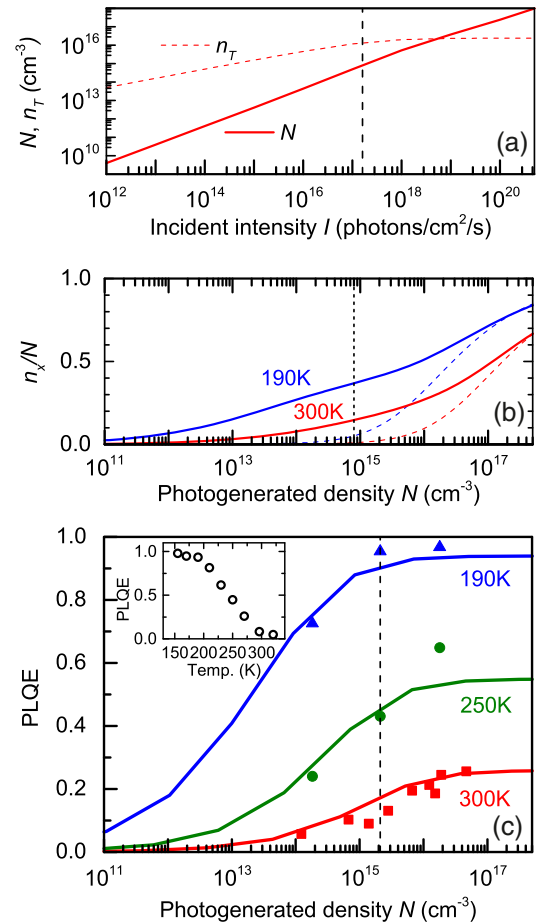


FIG. 3. (a) Concentration of filled traps  $n_T$  and of photogenerated species  $N$  at 300 K as a function of incident intensity  $I$ . The dashed line represents the incident absorbed flux for the perovskite under AM1.5  $100 \text{ mW cm}^{-2}$  irradiance ( $I \sim 1.6 \times 10^{17} \text{ cm}^{-2}/\text{s}$ ). (b) Fraction of excitons as a function of the total photogenerated concentration  $N$  at two temperatures. The dashed lines show the results using the Saha equation. The dotted line is an upper bound on charge density in a solar cell at open circuit. (c) PLQE data at 300 (squares), 250 (circles), and 190 K (triangles) with results from the model [Eq. (9)] overlaid by using PLQE and 300-K values for  $R_x = 3.2 \times 10^6 \text{ s}^{-1}$  and  $R_{eh} = 1.3 \times 10^{-10} \text{ cm}^3 \text{ s}^{-1}$  (see Supplemental Material Fig. S9 [31]). Inset: PLQE as a function of temperature through the range in which the perovskite crystal remains in the tetragonal phase (155–320 K) [21,47,48] under quasi-steady-state excitation corresponding to  $N \sim 2 \times 10^{15} \text{ cm}^{-3}$ .

the trap was due to an iodide vacancy) due to the exciton’s net charge neutrality, unless directly adjacent to a trap. We note that additional nonradiative pathways, such as non-radiative electron-hole or exciton recombination, must also occur at temperatures above 190 K, since the PLQE does not reach 100% at these temperatures even at high intensities when all of the traps are filled. We also note that a PLQE close to 100% in a polycrystalline semiconductor film simply prepared by solution casting is quite remarkable [20].

To calculate the PLQE, we consider the case of radiative decay of excitons and nonradiative decay of electrons and holes (PLQE<sub>x</sub>), the vice versa case (PLQE<sub>eh</sub>), or mixtures thereof. The PLQEs are defined as ratios of the radiative decay rate to the total decay rate:

$$\begin{aligned} \text{PLQE}_x &= \frac{n_x R_x}{n_x R_x + (N - n_x)[(N - n_x + n_T)R_{eh} + (N_T - n_T)R_{\text{pop}}]}, \\ \text{PLQE}_{eh} &= \frac{(N - n_x)n_T R_{eh}}{n_x R_x + (N - n_x)[(N - n_x + n_T)R_{eh} + (N_T - n_T)R_{\text{pop}}]}. \end{aligned} \quad (9)$$

These quantities represent the maximum PLQE values, because we assume that recombination through each respective channel ( $R_x$  or  $R_{eh}$ ) is purely radiative. Therefore, each quantity (or mixture thereof), whose shapes are indistinguishable, is scalable by a factor representing the radiative fraction of the respective decay channel(s).

We overlay these quantities on the experimental data in Fig. 3(c) by using the parameters ( $N_T$ ,  $R_{\text{pop}}$ , and  $\gamma_0$ ) obtained from the kinetic modeling and the values of  $n_T$  and  $N$  displayed in Fig. 3(a). The values of  $R_x$  and  $R_{eh}$  (Supplemental Material Fig. S9 [31]) are calculated by taking into account the experimental saturation values of the PLQE (0.25 for 300 K, 0.45–0.7 for 250 K, and 0.95 for 190 K), i.e., when all trap states are filled. The PLQE as a function of photogenerated density fits well to the experimental data. We note that the change in the rate constants  $R_x$  and  $R_{eh}$  with temperature are more physically realistic [50,51] when considering emission being preceded by the formation of an exciton (PLQE<sub>x</sub>), but this result does not exclude electron-hole recombination (PLQE<sub>eh</sub>) as an additional radiative pathway [31]. However, further work would be required to confirm this finding.

Based on these combined theoretical and experimental analyses, the following decay pathways emerge: When free electrons and holes meet, they may form an exciton, which will dissociate again into free electrons and holes with high probability. Occasionally, the excitons (or free electrons and holes) recombine radiatively, leading to photoluminescence, or nonradiatively. At higher temperatures and/or lower excitation fluences, the electrons and holes spend significantly more time as free charge than bound as excitons, and the free electrons are hence susceptible to becoming trapped in defect sites, resulting in nonradiative decay. As the photoexcited charge density increases and/or the temperature is reduced, the fractional time the charges spend bound as excitons increases, and the density of available trap states is reduced. Hence, the competition for radiative decay increases with respect to charge trapping, leading to increased PLQE.

### III. CONCLUSION

In summary, we have developed a theoretical model that is able to describe the dynamic interrelations between free

charges, excitons, and electronic subgap states for organic-inorganic metal-halide perovskites. The model reproduces the PL decays and PLQE trends. Importantly, the results suggest that high PLQE values can also be obtained at lower excitation fluences if the traps were otherwise filled or removed. In addition, the fraction of free charge carriers (versus excitons) under solar-cell working conditions would be increased from 90% towards 100% by reducing the photodoping density, presumed to occur due to the presence of subgap states. Future work should therefore concentrate on methods to switch off the subgap non-radiative pathways either by preventing their formation or by filling these states through selective doping or by chemically passivating the vacancies. This work would not only lead to solar cells with fewer losses, where all recombination is radiative [30], but also open up the possibility of using three-dimensional perovskites as highly efficient light-emitting devices.

### ACKNOWLEDGMENTS

The research leading to these results has received funding from the European Union Seventh Framework Program [FP7/2007-2013] under Grant Agreement No. 604032 of the MESO project. S. D. S. thanks Worcester College, Oxford, for additional financial support. T. L. acknowledges funding from the European Union Seventh Framework Program [FP7/2007-2013] under Grant Agreement No. 316494. A. G., H. J. S., and V. M. B. acknowledge the support of Oxford Martin School. A. G. is supported by a Reintegration Grant under EC Framework VII. The authors thank Elizabeth Parrot and Annamaria Petrozza for useful discussion.

- 
- [1] G. Hodes, Perovskite-based solar cells, *Science* **342**, 317 (2013).
  - [2] H. J. Snaith, Perovskites: The emergence of a new era for low-cost, high-efficiency solar cells, *J. Phys. Chem. Lett.* **4**, 3623 (2013).
  - [3] A. Kojima, K. Teshima, Y. Shirai, and T. Miyasaka, Organometal halide perovskites as visible-light sensitizers for photovoltaic cells, *J. Am. Chem. Soc.* **131**, 6050 (2009).

- [4] M. M. Lee, J. Teuscher, T. Miyasaka, T. N. Murakami, and H. J. Snaith, Efficient hybrid solar cells based on meso-superstructured organometal halide perovskites, *Science* **338**, 643 (2012).
- [5] S. D. Stranks, G. E. Eperon, G. Grancini, C. Menelaou, M. J. Alcocer, T. Leijtens, L. M. Herz, A. Petrozza, and H. J. Snaith, Electron-hole diffusion lengths exceeding 1 micrometer in an organometal trihalide perovskite absorber, *Science* **342**, 341 (2013).
- [6] E. Edri, S. Kirmayer, S. Mukhopadhyay, K. Gartsman, G. Hodes, and D. Cahen, Elucidating the charge carrier separation and working mechanism of CH<sub>3</sub>NH<sub>3</sub>PbI<sub>3</sub>-xCl<sub>x</sub> perovskite solar cells, *Nat. Commun.* **5**, 3461 (2014).
- [7] H.-S. Kim *et al.*, Lead iodide perovskite sensitized all-solid-state submicron thin film mesoscopic solar cell with efficiency exceeding 9%, *Sci. Rep.* **2**, 591 (2012).
- [8] J. Burschka, N. Pellet, S. J. Moon, R. Humphry-Baker, P. Gao, M. K. Nazeeruddin, and M. Grätzel, Sequential deposition as a route to high-performance perovskite-sensitized solar cells, *Nature (London)* **499**, 316 (2013).
- [9] K. Wojciechowski, M. Saliba, T. Leijtens, A. Abate, and H. J. Snaith, Sub-150 °C processed meso-superstructured perovskite solar cells with enhanced efficiency, *Energy Environ. Sci.* **7**, 1142 (2014).
- [10] N. J. Jeon, J. H. Noh, Y. C. Kim, W. S. Yang, S. Ryu, and S. I. Seok, Solvent engineering for high-performance inorganic-organic hybrid perovskite solar cells, *Nat. Mater.* **13**, 897 (2014).
- [11] G. E. Eperon, V. M. Burlakov, P. Docampo, A. Goriely, and H. J. Snaith, Morphological control for high performance, solution-processed planar heterojunction perovskite solar cells, *Adv. Funct. Mater.* **24**, 151 (2014).
- [12] J. M. Ball, M. M. Lee, A. Hey, and H. J. Snaith, Low-temperature processed meso-superstructured to thin-film perovskite solar cells, *Energy Environ. Sci.* **6**, 1739 (2013).
- [13] M. Liu, M. B. Johnston, and H. J. Snaith, Efficient planar heterojunction perovskite solar cells by vapour deposition, *Nature (London)* **501**, 395 (2013).
- [14] O. Malinkiewicz, A. Yella, Y. H. Lee, G. M. Espallargas, M. Grätzel, M. K. Nazeeruddin, and H. J. Bolink, Perovskite solar cells employing organic charge-transport layers, *Nat. Photonics* **8**, 128 (2014).
- [15] D. Liu and T. L. Kelly, Perovskite solar cells with a planar heterojunction structure prepared using room-temperature solution processing techniques, *Nat. Photonics* **8**, 133 (2014).
- [16] P. Docampo, J. M. Ball, M. Darwich, G. E. Eperon, and H. J. Snaith, Efficient organometal trihalide perovskite planar-heterojunction solar cells on flexible polymer substrates, *Nat. Commun.* **4**, 2761 (2013).
- [17] H. Zhou, Q. Chen, G. Li, S. Luo, T.-b. Song, H.-S. Duan, Z. Hong, J. You, Y. Liu, and Y. Yang, Interface engineering of highly efficient perovskite solar cells, *Science* **345**, 542 (2014).
- [18] G. Xing, N. Mathews, S. Sun, S. S. Lim, Y. M. Lam, M. Grätzel, S. Mhaisalkar, and T. C. Sum, Long-range balanced electron- and hole-transport lengths in organic-inorganic CH<sub>3</sub>NH<sub>3</sub>PbI<sub>3</sub>, *Science* **342**, 344 (2013).
- [19] H.-S. Kim, I. Mora-Sero, V. Gonzalez-Pedro, F. Fabregat-Santiago, E. J. Juarez-Perez, N.-G. Park, and J. Bisquert, Mechanism of carrier accumulation in perovskite thin-absorber solar cells, *Nat. Commun.* **4**, 2242 (2013).
- [20] F. Deschler *et al.*, High photoluminescence efficiency and optically pumped lasing in solution-processed mixed halide perovskite semiconductors, *J. Phys. Chem. Lett.* **5**, 1421 (2014).
- [21] V. D'Innocenzo, G. Grancini, M. J. Alcocer, A. R. Kandada, S. D. Stranks, M. M. Lee, G. Lanzani, H. J. Snaith, and A. Petrozza, Excitons versus free charges in organo-lead trihalide perovskites, *Nat. Commun.* **5**, 3586 (2014).
- [22] C. Wehrenfennig, M. Liu, H. J. Snaith, M. B. Johnston, and L. M. Herz, Homogeneous emission line broadening in the organo lead halide perovskite CH<sub>3</sub>NH<sub>3</sub>PbI<sub>3</sub>-xCl<sub>x</sub>, *J. Phys. Chem. Lett.* **5**, 1300 (2014).
- [23] G. Xing, N. Mathews, S. S. Lim, N. Yantara, X. Liu, D. Sabba, M. Grätzel, S. Mhaisalkar, and T. C. Sum, Low-temperature solution-processed wavelength-tunable perovskites for lasing, *Nat. Mater.* **13**, 476 (2014).
- [24] C. Wehrenfennig, G. E. Eperon, M. B. Johnston, H. J. Snaith, and L. M. Herz, High charge carrier mobilities and lifetimes in organolead trihalide perovskites, *Adv. Mater.* **26**, 1584 (2014).
- [25] A. Marchioro, J. Teuscher, D. Friedrich, M. Kunst, R. van de Krol, T. Moehl, M. Grätzel, and J. E. Moser, Unravelling the mechanism of photoinduced charge transfer processes in lead iodide perovskite solar cells, *Nat. Photonics* **8**, 250 (2014).
- [26] C. S. Ponseca, Jr. *et al.*, Organometal halide perovskite solar cell materials rationalized: Ultrafast charge generation, high and microsecond-long balanced mobilities, and slow recombination, *J. Am. Chem. Soc.* **136**, 5189 (2014).
- [27] P. Langevin, Recombination and ion mobility in gases, *Ann. Chim. Phys.* **28**, 433 (1903).
- [28] P. K. Nayak, K. L. Narasimhan, and D. Cahen, Separating charges at organic interfaces: Effects of disorder, hot states, and electric field, *J. Phys. Chem. Lett.* **4**, 1707 (2013).
- [29] L. C. Schmidt, A. Pertegas, S. Gonzalez-Carrero, O. Malinkiewicz, S. Agouram, G. Minguez Espallargas, H. J. Bolink, R. E. Galian, and J. Perez-Prieto, Nontemplate synthesis of CH<sub>3</sub>NH<sub>3</sub>PbBr<sub>3</sub> perovskite nanoparticles, *J. Am. Chem. Soc.* **136**, 850 (2014).
- [30] O. D. Miller, E. Yablonovitch, and S. R. Kurtz, Strong internal and external luminescence as solar cells approach the Shockley-Queisser limit, *IEEE J. Photovoltaics* **2**, 303 (2012).
- [31] See Supplemental Material at <http://link.aps.org/supplemental/10.1103/PhysRevApplied.2.034007> for full experimental methods, detailed mathematical workings, and additional modeling results for different temperatures and binding energies and low-temperature PL measurements.
- [32] B. C. O'Regan and F. Lenzmann, Charge transport and recombination in a nanoscale interpenetrating network of n-type and p-type semiconductors: Transient photocurrent and photovoltage studies of TiO<sub>2</sub>/dye/CuSCN photovoltaic cells, *J. Phys. Chem. B* **108**, 4342 (2004).
- [33] A. Abrusci, S. D. Stranks, P. Docampo, H.-L. Yip, A. K. Y. Jen, and H. J. Snaith, High-performance perovskite-polymer hybrid solar cells via electronic coupling with fullerene monolayers, *Nano Lett.* **13**, 3124 (2013).
- [34] T. Ishihara, Optical properties of PbI<sub>2</sub>-based perovskite structures, *J. Lumin.* **60–61**, 269 (1994).

- [35] K. Tanaka, T. Takahashi, T. Ban, T. Kondo, K. Uchida, and N. Miura, Comparative study on the excitons in lead-halide-based perovskite-type crystals  $\text{CH}_3\text{NH}_3\text{PbBr}_3$   $\text{CH}_3\text{NH}_3\text{PbI}_3$ , *Solid State Commun.* **127**, 619 (2003).
- [36] M. Hirasawa, T. Ishihara, T. Goto, K. Uchida, and N. Miura, Magnetoabsorption of the lowest exciton in perovskite-type compound  $(\text{CH}_3\text{NH}_3)\text{PbI}_3$ , *Physica (Amsterdam)* **201B**, 427 (1994).
- [37] V. Perebeinos and P. Avouris, Exciton ionization, Franz-Keldysh, and Stark effects in carbon nanotubes, *Nano Lett.* **7**, 609 (2007).
- [38] J. Szczytko, L. Kappei, J. Berney, F. Morier-Genoud, M. T. Portella-Oberli, and B. Deveaud, Determination of the exciton formation in quantum wells from time-resolved interband luminescence, *Phys. Rev. Lett.* **93**, 137401 (2004).
- [39] S. W. Koch, M. Kira, G. Khitrova, and H. M. Gibbs, Semiconductor excitons in new light, *Nat. Mater.* **5**, 523 (2006).
- [40] J. Even, L. Pedesseau, and C. Katan, Analysis of multivalley and multibandgap absorption and enhancement of free carriers related to exciton screening in hybrid perovskites, *J. Phys. Chem. C* **118**, 11566 (2014).
- [41] M. N. Saha, On a physical theory of stellar spectra, *Proc. R. Soc. A* **99**, 135 (1921).
- [42] M. Graetzel, R. A. J. Janssen, D. B. Mitzi, and E. H. Sargent, Materials interface engineering for solution-processed photovoltaics, *Nature (London)* **488**, 304 (2012).
- [43] Q. Cao, O. Gunawan, M. Copel, K. B. Reuter, S. J. Chey, V. R. Deline, and D. B. Mitzi, Defects in  $\text{Cu}(\text{In,Ga})\text{Se}_2$  chalcopyrite semiconductors: A comparative study of material properties, defect states, and photovoltaic performance, *Adv. Energy Mater.* **1**, 845 (2011).
- [44] D. M. Smyth, Defects and order in perovskite-related oxides, *Annu. Rev. Mater. Sci.* **15**, 329 (1985).
- [45] W.-J. Yin, T. Shi, and Y. Yan, Unusual defect physics in  $\text{CH}_3\text{NH}_3\text{PbI}_3$  perovskite solar cell absorber, *Appl. Phys. Lett.* **104**, 063903 (2014).
- [46] I. A. Shkrob and T. W. Marin, Charge trapping in photo-voltaically active perovskites and related halogenoplumbate compounds, *J. Phys. Chem. Lett.* **5**, 1066 (2014).
- [47] T. Ishihara, J. Takahashi, and T. Goto, Optical properties due to electronic transitions in two-dimensional semiconductors, *Phys. Rev. B* **42**, 11099 (1990).
- [48] T. Baikie, Y. N. Fang, J. M. Kadro, M. Schreyer, F. X. Wei, S. G. Mhaisalkar, M. Graetzel, and T. J. White, Synthesis and crystal chemistry of the hybrid perovskite  $(\text{CH}_3\text{NH}_3)\text{PbI}_3$  for solid-state sensitised solar cell applications, *J. Mater. Chem. A* **1**, 5628 (2013).
- [49] J. C. de Mello, H. F. Wittmann, and R. H. Friend, An improved experimental determination of external photoluminescence quantum efficiency, *Adv. Mater.* **9**, 230 (1997).
- [50] Y. P. Varshni, Band-to-band radiative recombination in groups IV, VI, and III-V semiconductors (I), *Phys. Status Solidi (b)* **19**, 459 (1967).
- [51] H. Schlangenotto, H. Maeder, and W. Gerlach, Temperature dependence of the radiative recombination coefficient in silicon, *Phys. Status Solidi (a)* **21**, 357 (1974).